Femtosecond Transient Absorption of Zinc Porphyrins with Oligo(phenylethylnyl) Linkers in Solution and on TiO_2 Films†

Chih-Wei Chang,‡ Liyang Luo,‡,§ Chung-Kung Chou,‡ Chen-Fu Lo,|| Ching-Yao Lin,|| Chen-Shiung Hung,§ Yuan-Pern Lee,‡ and Eric Wei-Guang Diau*,‡

Department of Applied Chemistry and Institute of Molecular Science, National Chiao Tung University, Hsinchu 300, Taiwan, Institute of Chemistry, Academia Sinica, Taipei 115, Taiwan, and Department of Applied Chemistry, National Chi Nan University, Puli, Nantou 545, Taiwan

Received: December 2, 2008; Revised Manuscript Received: February 12, 2009

We measured femtosecond transient absorption of dye solutions and TiO_2 films sensitized with two zinc porphyrins (PE1 and PE4) to investigate the interfacial dynamics of electron transfer in relation to the dependence of cell performance on the length of the linker (Lin, C.-Y.; Lo, C.-F.; Luo, L.; Lu, H.-P.; Hung, C.-S.; Diau, E. W.-G. *J. Phys. Chem. C* **2009**, *113*, 755−764). For both porphyrins adsorbed on TiO_2 films with S_1 excitation (λ_{ex} = 620 nm), the transient absorption kinetics probed at 630 nm and 4.9 μm are complementary to each other because only the excited-state and ground-state species were observed at 630 nm whereas only the charge-separation intermediates were observed at 4.9 μm. The transient of the PE1/TiO_2 film shows a single exponential decay with a large offset, whereas the transient of the PE4/TiO_2 film displays a biexponential decay with a small offset. Because of the existence of an additional ps component, the amount of free delocalized electrons (offset signal) in PE4/TiO_2 is smaller than that in PE1/TiO_2. Our results imply that back electron transfer at the TiO_2/dye interface is an important factor to be considered to account for the cell performance of a device.

1. Introduction

Dye-sensitized solar cells (DSSC) have attracted much attention due to the problem of global warming and the demand of environmentally responsible energy sources.[1] The greatest efficiency (η) of conversion of light to electricity is achieved with ruthenium polypyridine complexes (e.g., $Ru(dcbpy)_2(NCS)_2$, abbreviated N_3).[2] The interfacial electron transfer (IET), including both electron injection (EI) and back electron transfer (BET), is critical to the overall efficiency of a DSSC.[3−7] Based on femtosecond (fs) transient absorption (TA), the IET dynamics of the N3/TiO_2 system have been extensively investigated.[4−6] Typical EI dynamics exhibit a biphasic nature: an ultrarapid component (<100 fs) accompanied by a ps component.[3,4] To rationalize the observed dynamics, a two-state relaxation model was proposed: the rapid component resulted from EI from the nonthermalized state, whereas the ∼ps component was attributed to EI from the relaxed excited state; the disparate rates of injection arose from the variation of the density of states of TiO_2 film with energy.[4,5] Lian and co-workers investigated the effect of electronic coupling between the dye and the TiO_2 surface, and reported the dynamics of electron transfer dependent on the bridge length of Re polypyridyl complexes.[5a,b] The results indicated that the EI rate decreases greatly with an insertion of $-CH_2-$ linking groups, because of deteriorated electronic coupling between the Re complexes and the TiO_2 film.[5a,b] The effects of pump photon density, environment of the sensitized films (whether solvent or air), and the parameters of film preparation were also tested.[6d] The results indicated that the EI dynamics varied significantly under a large density of pump photons, and the exposure of sensitized films to air caused the degradation of the dye molecules.[6d]

The BET of the N3/TiO_2 films typically occurs on a time scale of microseconds to milliseconds;[8−11] many factors such as pH, excitation intensity, electrolyte composition, and the application of an electrical bias on TiO_2 film affect this process.[8d,12] Beyond the traditional time scale of BET of ∼microseconds to ∼milliseconds, Ghosh and co-workers observed a sub-ps BET in catecholate binding molecules;[13] they proposed that the BET for electrons localized on Ti atoms is much more rapid than diffusion of electrons to the conduction band of TiO_2 film because of the superior electronic coupling between the localized electrons and the adsorbate cations. For localized electrons, an ultrarapid BET was expected; the delocalized electrons contributed the BET on the typical micro or millisecond scale.[13a]

The capability of porphyrins to absorb visible light in regions 400−450 nm (Soret or B band) and 500−700 nm (Q bands) makes these dyes prospectively efficient light-harvesting sensitizers.[3b,14−18] The cell performance of a DSSC based on a push−pull zinc porphyrin is reported to be comparable with that of a N3-based device, which makes this green dye attractive for DSSC applications.[18] Tachibana et al. reported the ultrarapid EI dynamics of porphyrin/TiO_2 systems resembling those of N3/TiO_2 films.[8c] The catecholate-binding porphyrins on TiO_2 films exhibited a sub-ps BET, with decreased efficiency of power conversion relative to the corresponding porphyrin-based DSSC.[13b] We reported[3a] the fs relaxation dynamics of a zinc porphyrin with one phenylethylnyl (PE) linker sensitized on nanoporous TiO_2 films. To assess the effect of the length of the linker on the photovoltaic performance of the device, we systematically designed porphyrin dyes from a porphyrin with one PE unit (abbreviated PE1, Chart 1) to a porphyrin with four

† Part of the "Hiroshi Masuhara Festschrift".

* Corresponding author. Fax: (886)-03-572-3764. E-mail: diau@mail.nctu.edu.tw.

‡ National Chiao Tung University.

§ Academia Sinica.

|| National Chi Nan University.

10.1021/jp810580u CCC: $40.75
Published on Web 03/26/2009

CHART 1: Molecular Structures of PE1 and PE4

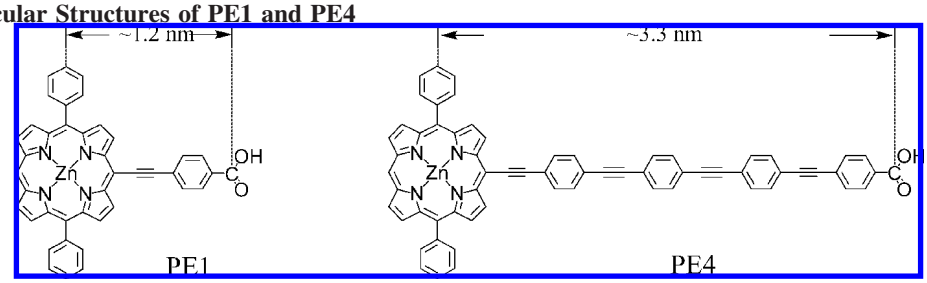

PE units (PE4, Chart 1); the cell performances of the devices decreased systematically from 2.5 ± 0.2% (PE1) to 0.25 ± 0.02% (PE4), whereas the EI dynamics of the corresponding dye/TiO_2 films were similar.[3b] Because the rate of EI of dyes with long links did not decrease to account for the systematic degradation of the cell performance with increasing length of the linker, other factors such as rate of the charge recombination should be considered.

We measured fs TA of dye solutions and on TiO_2 films sensitized with PE1 and PE4 to understand the factors governing the observed dependence of cell performance on the length of the link.[3b] Both solution and thin-film samples were excited at the maxima of the Soret band (λ_{ex} = 430 nm) and the Q(0,0) band (λ_{ex} = 620 nm); the TA spectra were probed with white-light generation. To improve the kinetic information for the thin-film samples, we detected at single wavelength in two spectral regions: (i) the ground-state bleaching kinetics were probed at 630 nm and the dye cationic states at 900 nm with a fs vis/NIR spectrometer; (ii) the electron-transport kinetics were monitored at 4.9 μm with a fs mid-IR spectrometer. Our results indicate that the kinetics of transfer of localized electrons in the PE1/TiO_2 film exhibit a single exponential decay whereas the decay in the PE4/TiO_2 film is biexponential with a rapid decay (or recovery) that is absent in the case of the PE1/TiO_2 film. Because of the rapid decay, the number of free delocalized electrons in PE4/TiO_2 is smaller than in PE1/TiO_2. These delocalized electrons produce an enhanced photocurrent in the device, yielding a superior efficiency of power conversion for PE1 than for PE4.

2. Results and Discussion

2.1. Relaxation Dynamics of PE1 in Solution. The steady-state absorption and emission spectra of PE1 in solution are reported elsewhere.[3] Briefly, PE1 absorbs light in the Soret and Q bands, due to transitions $S_0 \rightarrow S_2$ and the $S_0 \rightarrow S_1$, respectively. The maximum of the Soret band is at 439 nm, with the Q(0,0) band at 616 nm and Q(1,0) at 567 nm; the corresponding emission spectrum shows a mirror image of the Q bands.

After excitation at 430 and 620 nm, we probed the S_2 and S_1 relaxation dynamics of PE1 in solution with the fs pump−probe/TA technique; the TA spectra appear in Figure 1, panels a and b, respectively. Figure 2a−c shows detailed S_2 relaxation kinetics of the TA spectra at three representative probe wavelengths: 470, 625, and 700 nm, respectively; the S_1 relaxation kinetics that exhibit only offset signals are not discussed here. The transient at 470 nm (Figure 2a) is fitted with two components, the first decays in ~7 ps and the second rises also in ~7 ps. We assign the first component to both S_2 and hot S_1 species (indistinguishable in this detection window) decaying in ~7 ps to the cold S_1 species, and the second component to the cold S_1 species that was produced in ~7 ps; this relaxation coefficient is consistent with the fluorescence transient in our previous work showing a risetime coefficient 8.5 ps.[3] The transient at 700 nm (Figure 2c) is also fitted with two components, the first decaying in ~0.7 ps and the second persisting as an offset observed for some 30 ps. Because the internal conversion $S_2 \rightarrow S_1$ occurs in 0.91 ps as probed with fluorescence decay,[3] we assign the first component to the S_2 state and the offset component to both hot and cold S_1 species that were indistinguishable in the detection window at greater wavelengths. The S_2 TA kinetics probed at 625 nm (Figure 2b) seem more complicated than the other two cases because of the involvement of both the depleted transient absorption and the stimulated transient emission signals discussed in the following.

As shown in Figure 1, all temporally dependent TA spectra at positive delays feature a strong absorption with maximum at ~470 nm. Whereas these positive bands, due to absorption by populations in excited states, diminish along the wavelength axis toward the near-infrared, two negative TA signals about ~600 nm oppositely mimic the ground-state absorption of the Q-bands, shown as gray dashed curves in Figure 1. As a result, the negative absorbance shown in the temporally resolved TA spectra was due to the $S_0 \rightarrow S_1$ absorption (probe) when the S_0 population was depleted after excitation (pump). To clarify the negative TA signals shown in Figure 1a, we show five temporally resolved spectra (λ_{ex} = 430 nm) separately in Figure 3a−e. At time zero, the bleaching ground-state absorption appears at 616 and 565 nm (Figure 3b), which match exactly the normal ground-state absorption features shown in Figure 3a (gray solid curve), but we observed that the TA signals gradually shifted toward greater wavelengths as the delay increased from 500 fs (Figure 3c) to 50 ps (Figure 3e). At 50 ps, the position of the major negative feature was red-shifted to ~620 nm, which is near the Q(0,0) band in the steady-state emission spectrum shown as a gray dashed curve in Figure 3a; for clarity, two vertical gray dotted lines are indicated in Figure 3 to represent the positions of the steady-state absorption and emission spectral features for comparison. A new negative band was produced about 680 nm, which is near the Q(0,1) band of the steady-state emission spectrum. These results thus indicate that stimulated emission of the $S_1 \rightarrow S_0$ transition was observed also in the TA spectra, as well as the depleted absorption of the $S_0 \rightarrow S_1$ transition.

2.2. Transient Absorption Spectra on TiO_2 Films. Figure 4, panels a and b, shows absorption spectra of PE1 and PE4 adsorbed on TiO_2 films, respectively; the spectra of solution samples ($c = 1 \times 10^{-4}$ M) are shown as dashed curves for comparison. Spectra normalized at the Q(0,0) band are shown in the insets. Both Soret and Q bands are significantly broadened for thin-film samples through the formation of aggregates on the TiO_2 surface.[3,19] The slight bathochromic shift of the absorption spectra indicates the formation of charge-transfer

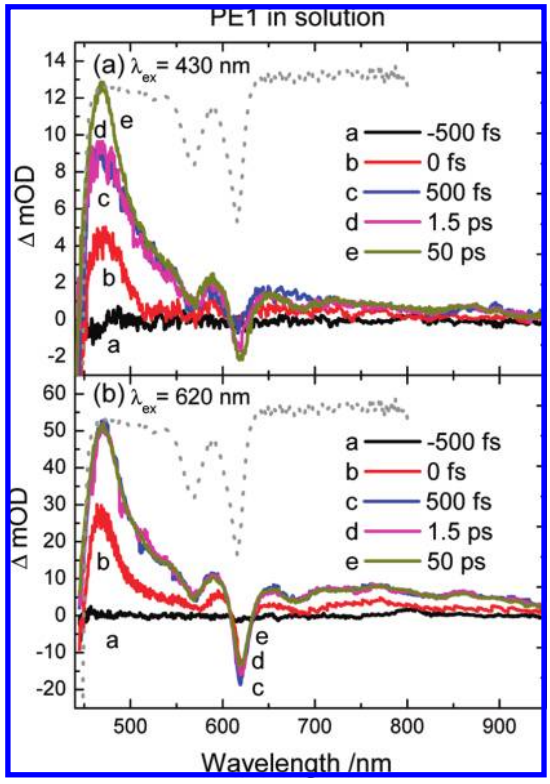

Figure 1. Transient absorption spectra of PE1 in THF/CH_2Cl_2 solution with excitation wavelengths (a) 430 and (b) 620 nm, with various delays as indicated for curves a−e. The inverse steady-state absorption spectra are indicated as gray dotted curves for comparison.

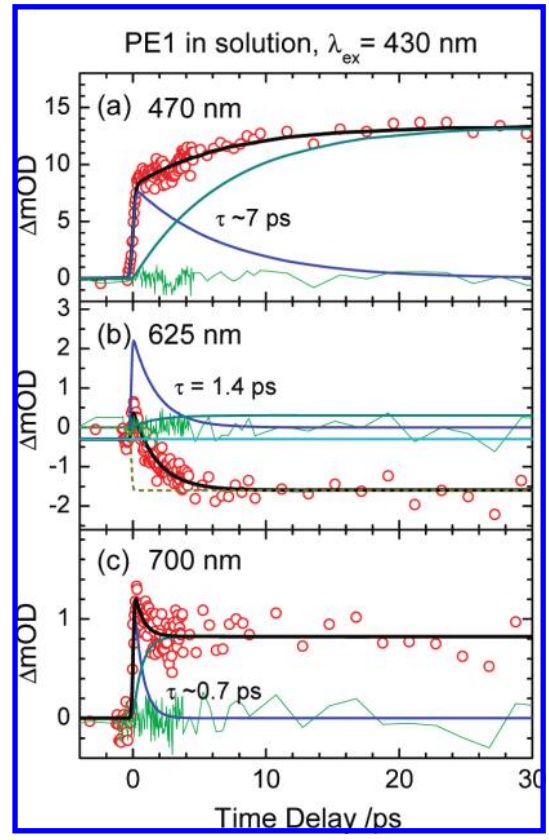

Figure 2. Three typical femtosecond transient absorption temporal profiles of PE1 in THF/CH_2Cl_2 solution obtained at probe wavelengths (a) 470, (b) 625, and (c) 700 nm. Open circles denote raw data and solid curves represent theoretical fits with convolution of the laser pulse; the residues between data and the fits are shown as thin green solid traces.

complexes between porphyrins and TiO_2 nanoparticles.[13b] The tail in the absorption of PE1/TiO_2 film is attributed to Mie scattering of the TiO_2 nanoparticles.[1c]

The TA spectra of the PE1/TiO_2 film upon excitation at S_2 (λ_{ex} = 430 nm) and S_1 (λ_{ex} = 620 nm) appear in Figures 5 and 6, respectively. The profiles of the TA spectra of these thin films are similar to those of the solution samples (Figure 1) with two absorption bands downward at ~570 and ~620 nm oppositely mimicking the ground-state absorptions (Figure 4), but three additional features appear in the TA profiles of the thin-film samples: the absorbance about 500 nm of the thin-film samples is much smaller than that of solution samples; a broad absorption band about 900 nm was absent in the TA profiles of the solution samples, and the TA profiles of thin-film samples decay to a small offset level whereas those of the solution samples persist longer. We thus propose that the thin-film samples undergo additional relaxations. Other measurements of fs fluorescence decay[3] indicated that the populations of PE1 in excited states on TiO_2 films were quenched within 10 ps because of ultrarapid IET and aggregate-induced energy transfer, but the observed transient signals of the thin-film samples endure even at 50 ps; the TA signals must hence be contributed by other transient species, i.e., electrons in the conduction band of TiO_2 or oxidized dye cationic species after charge separation. The TA signals of electrons on the TiO_2 conduction band have been assigned,[13] and electrons trapped on a TiO_2 surface are well-known to exhibit a broad absorption in the visible, near-IR, and mid-IR regions.[5,20,21] To obtain information about the dynamics in PE1/TiO_2 films, we measured the transients at four excitation wavelengths, with the probe wavelength fixed at 900 nm corresponding to the absorption of the PE1 excited-state as well as cationic species (evidence for oxidized PE1 species is given in the Supporting Information, Figure S1).

2.3. Transient Absorption Decays of PE1/TiO_2 Film at Varied Excitations. Figure 7 shows the TA decays of the PE1/TiO_2 film at λ_{ex}/nm = 430, 620, and 700, respectively, with all transients fitted with three decay components and one offset in a parallel kinetic model (Supporting Information, Figures S2−S4). We summarize our assignment for the observed relaxation processes as follows. The first decay component (τ_1 ~0.3 ps in Figure S1 and ~1 ps in Figure S4) is attributed to the excited-state species undergoing EI; the second decay component (τ_2 ~3 ps in Figures S2 and S3 and ~5 ps in Figure S4) is attributed to the electron cooling in TiO_2; and the third decay component (τ_3 = 20−30 ps in Figures S2−S4) is attributed to the cationic species undergoing BET.

The time coefficients are similar for the transients with λ_{ex} = 430 and 620 nm, but those obtained at λ_{ex} = 700 nm are significantly smaller than the others. This result conforms with the model that Marcus and co-workers proposed,[5e,22] in which the energy dependence of the rate of electron injection is significant only for the excited-state of the dye near the conduction band edge of TiO_2.[5c,e] The relative amplitude of the offset decreases systematically as the excitation wavelength increases from 430 to 700 nm. As the offset is reasonably assigned to delocalized electrons in TiO_2,[13] our result implies simply that electron delocalization becomes more efficient for the electrons with greater available energy (smaller λ_{ex}). The electronic motion on TiO_2 is well described with a model of continuous-time random walk (CTRW),[23,24] in which the

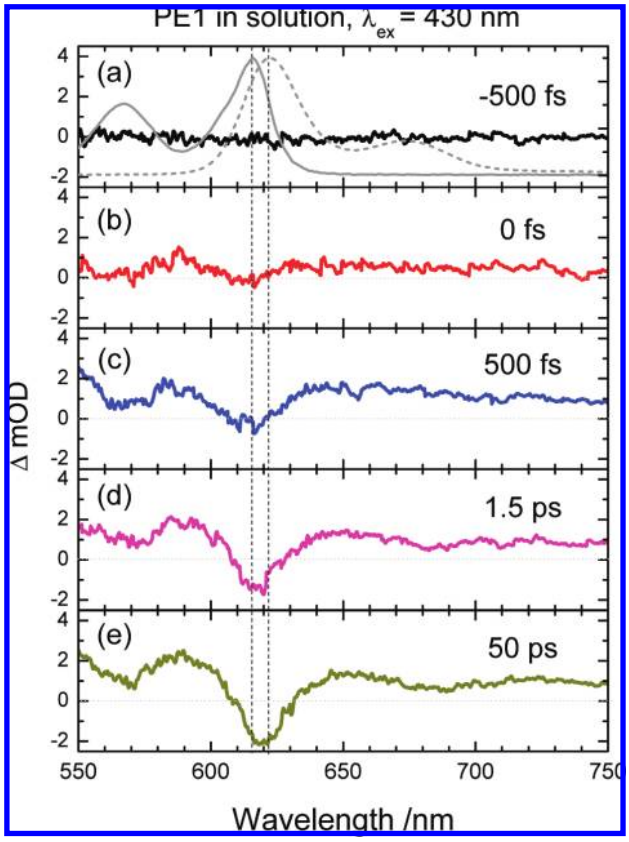

Figure 3. Transient absorption spectra obtained at delays (a) −500 fs, (b) 0 fs, (c) +500 fs, (d) +1.5 ps, and (e) +50 ps. In part a, the steady-state UV/vis and emission spectra are indicated as gray solid and dashed curves, respectively. For clarity, the maxima of absorption and emission of band Q(0,0) are indicated as vertical black dashed lines.

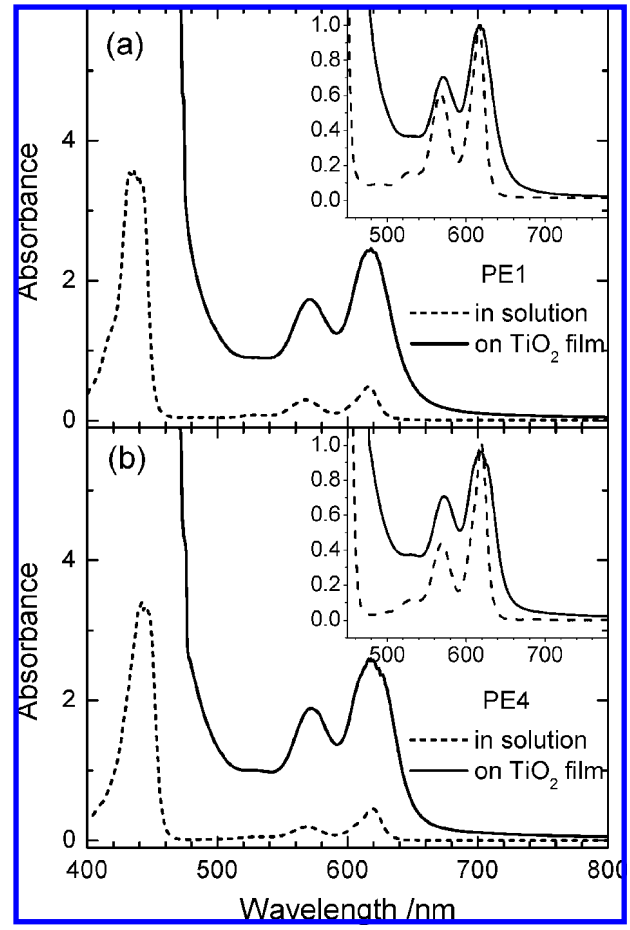

Figure 4. Steady-state UV/vis absorption spectra of (a) PE1 and (b) PE4 in THF/CH_2Cl_2 solution and on TiO_2 films as indicated. The insets show the spectra normalized according to the Q (0,0) band.

electrons move through the lattice of trapping states in TiO_2. Once the electrons become trapped, their detrapping requires an activation energy for the trapping sites currently occupied.[24] According to this model, we expect a greater rate of electron delocalization for electrons with greater energy, thus producing greater offset signals, in agreement with our experimental results.

2.4. Transient Absorption Kinetics of PE1/TiO_2 and PE4/TiO_2 Films Probed at 620 nm and 4.9 μm. To improve the quality of data for the TA kinetics and to understand further the mechanism of interfacial electron transfer, we measured single-wavelength TA for PE1 and PE4 adsorbed on TiO_2 films with S_1 excitation (λ_{ex} = 620 nm) at two probe wavelengths, λ_{pr} = 630 nm and 4.9 μm, which correspond to detection of the depleted ground-state and electrons in the TiO_2 conduction band, respectively. The results for the PE1/TiO_2 and PE4/TiO_2 films appear in Figure 8a−d. For each transient, the temporal coefficients were obtained on fitting the curve of the fs TA data with a composite parallel/consecutive kinetic model (detailed in Supporting Information, Figures S5 and S6):

$$A \xrightarrow{\tau_1} B \xrightarrow{\tau_2} C$$

$$A \xrightarrow{\tau_1} B' \xrightarrow{\tau_3} C$$

$$A \xrightarrow{\tau_1} B'' \xrightarrow{\infty} C$$

In this kinetic model, A represents the excited-state species produced upon photoexcitation, B, B', and B″ represent three charge-separation intermediates produced from A, and C represents the ground-state species reformed via charge recombination. The B'' intermediate did not return to the stable C species within the observed time window.

For the transient absorption probed at 630 nm (Figure 8, panels a and b), the negative signals at $t = 0$ reflect the depletion of the ground-state population ($I_{pr} > I_{ref}$ or $\Delta OD < 0$). At a positive delay, the recovery of the depleted ground-state population (C) provides crucial information about the relaxation of the excited-state species to the ground state. The TA signals subsequently returned to a level (denoted Δ) below the background because only part of the ground-state population recovered on that time scale (t < 200 ps). The depleted TA signals involved, however, a decay feature in the sub-ps region that was fitted on including the contribution of the A component (see Supporting Information, Figures S5 and S6). As a result, both excited-state species (A) and ground-state species (C) were bright whereas the charge-separation intermediates ($B/B'/B''$) might be dark (insensitive to the probe) when probed at 630 nm. For the PE1/TiO_2 film, the recovery kinetics are described with a single exponential decay (τ_2 = 20 ps), whereas for the PE4/TiO_2 film a biexponential function (τ_2 = 60 ps, τ_3 = 4.3 ps) was required. In both cases the recovery transients involve a rapid component (τ_1 ~250 fs, shown in insets of Figure 8, panels a and b) that corresponds to electron injection from dye to TiO_2. The electron cooling in TiO_2 was not observed in this detection window.

In contrast with the results observed at 630 nm, the TA signals probed at 4.9 μm were all positive because the ground-state

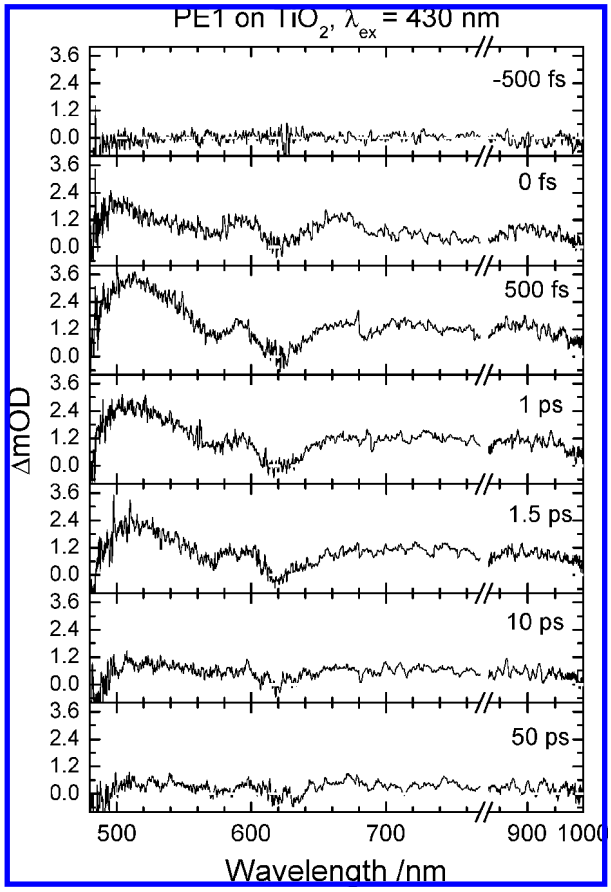

Figure 5. Transient absorption spectra of PE1 on a TiO_2 film with λ_{ex} = 430 nm and various delays as indicated.

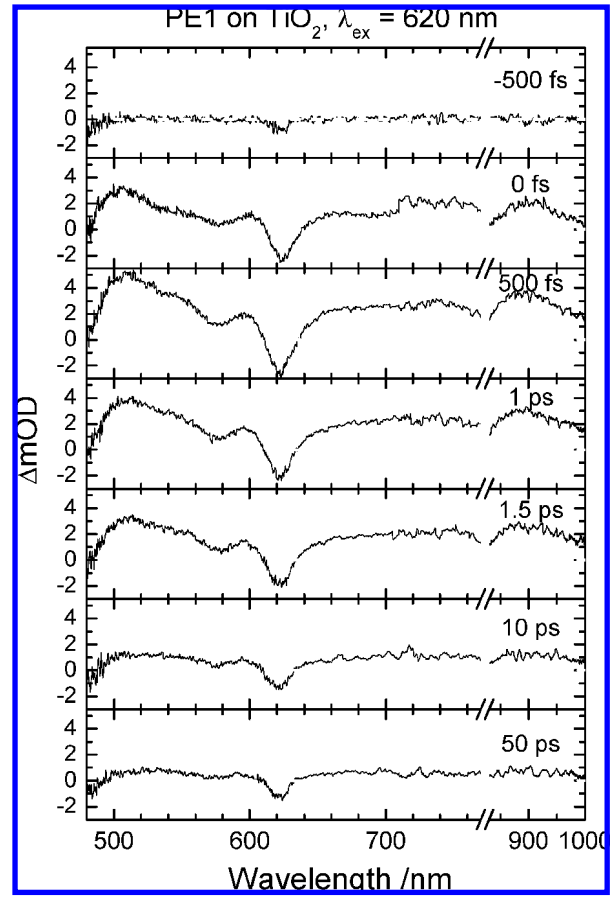

Figure 6. Transient absorption spectra of PE1 on a TiO_2 film with λ_{ex} = 620 nm and various delays as indicated.

species (*C*) were insensitive to the probe. The rising feature shown in the insets of Figure 8, panels c and d, further excludes a contribution of the excited-state species (*A*). Only the charge-separation intermediates (*B*/*B*′/*B*″) were thus probed with the mid-IR fs laser pulse. The rise coefficients (~200 fs) observed at 4.9 μm are similar to the decay coefficients (~250 fs) observed at 630 and 900 nm (Figure 7), confirming that electron injection from the dye to TiO_2 was ultarapid.[3] Similar to those observed at 630 nm, the transient of the PE1/TiO_2 film at 4.9 μm shows a single exponential decay (τ_2 = 40 ps), whereas the transient of the PE4/TiO_2 film at 4.9 μm displays a biexponential decay (τ_2 = 42 ps, τ_3 = 2.3 ps) with a smaller Δ value. A mechanism to rationalize the observed fs relaxation kinetics of the thin-film samples is explained in the next section.

2.5. Mechanism of Electron Transfer. The recovery of the bleaching signals provides direct evidence for the BET dynamics of porphyrins on TiO_2 films. According to the model proposed by Ghosh and co-workers,[13] the 20-ps component was attributed to localized electrons undergoing BET and the offset was assigned to delocalized electrons persisting longer. In our case, the TA kinetics probed at 630 nm and 4.9 μm are mutually complementary; the assignment for the charge-separation intermediates is hence straightforward. As detection in the mid-IR region is more sensitive to unbound electrons,[5] the decays of transients probed at 4.9 μm reflect the charge recombination between the dye cations and electrons localized near the cations on the TiO_2 surface.[13] The offset signals (Δ) in all cases represent the proportion of free delocalized electrons in TiO_2 that require a much greater duration to complete the charge recombination.[8] The observed charge-carrier dynamics of the PE1/TiO_2 and PE4/TiO_2 films occur according to the following mechanism.

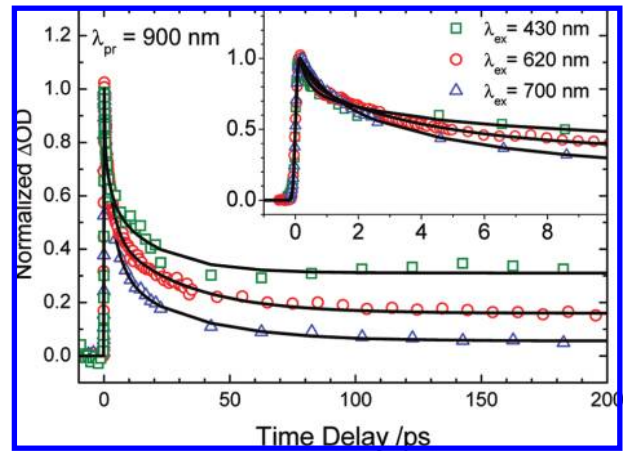

Figure 7. Single-wavelength transient absorption decays of PE1 on a TiO_2 film with λ_{pr}/nm = 900 and λ_{ex}/nm = 430, 620, and 700. Open symbols denote raw data and solid curves represent theoretical fits with convolution of the laser pulse. The inset shows the corresponding transients at a brief duration.

Upon excitation at 620 nm, only the ground-state porphyrin (ZnP) of the ZnP−TiO_2 composite becomes excited to its first singlet excited state (ZnP*). Because the time scale for electron injection from ZnP* to TiO_2 is much smaller than that for the relaxation of electronic energy of ZnP*,[3] charge separation produced an electron−hole pair ($ZnP^{\bullet+}-TiO_2^{\bullet-}$); this process occurred on the observed 200−300 fs in both PE1/TiO_2 and PE4/TiO_2 films. The electrons weakly bound in $ZnP^{\bullet+}-TiO_2^{\bullet-}$ might be delocalized to form free electrons inside TiO_2 ($TiO_2^{\bullet-}$). Charge recombination might occur for the localized electrons

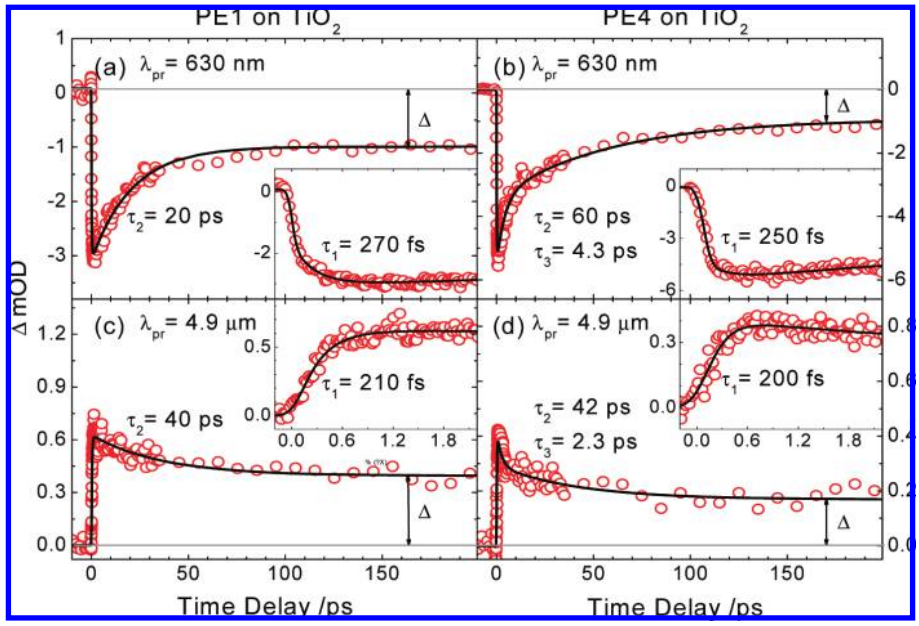

Figure 8. Femtosecond transient absorption profiles obtained with excitation at 620 nm for a PE1/TiO_2 film probed at (a) 630 nm and (c) 4.9 μm, and for a PE4/TiO_2 film probed at (b) 630 nm and (d) 4.9 μm; the data (circles) were fitted (solid curves) according to an appropriate kinetic model with the indicated time coefficients. The insets show the corresponding transients at a brief duration. The offset of each transient is indicated by Δ.

SCHEME 1: Schematic Representation of through-Bond and through-Space Back Electron Transfer (BET) Occurring at the Dye/TiO_2 Interface

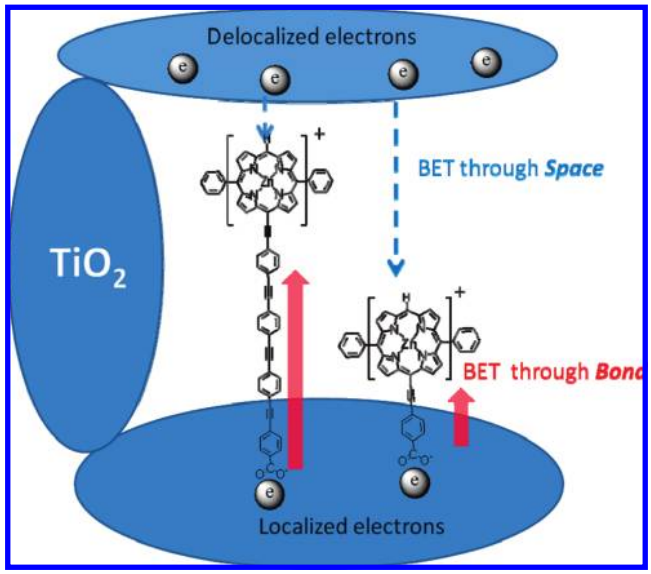

(e^- in $ZnP^{\bullet+}-TiO_2^{\bullet-}$)undergoing interfacial electron transfer through the PE link. For the PE1/TiO_2 film, only intermediates *B* and *B″* are involved, in which the former and the latter represent localized electrons and delocalized electrons, respectively. For the PE4/TiO_2 film, however, an additional *B′* species was involved to account for the ps component that was absent from the transient of the PE1/TiO_2 film.

We rationalize the dependence of the cell performance on the length of the linker[3b] with the observed kinetics of interfacial electron transfer as follows. The electron transfer of the localized electrons in PE1/TiO_2 is single-exponential whereas that in PE4/TiO_2 is biexponential with a rapid decay (or recovery) that was absent in the case of PE1/TiO_2. Because of the rapid decay, the concentration of free delocalized electrons (Δ) in PE4/TiO_2 is smaller than that in PE1/TiO_2, which is unambiguously shown

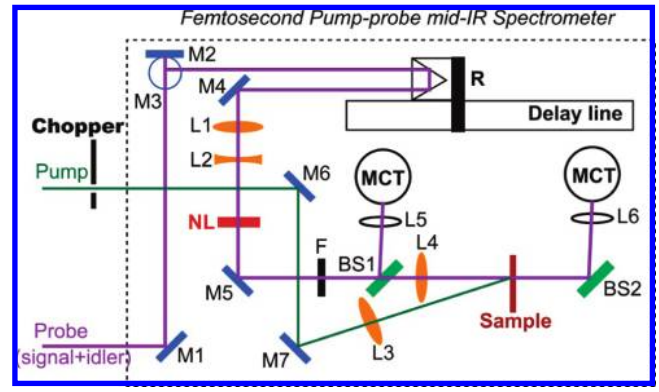

Figure 9. Optical layout of a femtosecond mid-IR transient absorption system. M1-M7: mirrors; BS1-BS2: beam splitter; PD: photodiode; L1-L6: lenses Pl: polarizer; F: color filter; R: retro-reflector; NL: nonlinear crystal ($AgGaS_2$) for difference-frequency generation; MCT: HgCdTe detector cooled with liquid nitrogen.

in Figure 8. Subsequently, more delocalized electrons are expected to produce higher photocurrent in the device, and this is consistent with the observed cell performance of the device showing a superior efficiency of power conversion for PE1 than for PE4.[3b]

Why do the dye molecules with a longer π-conjugated linker on TiO_2 show more rapid back electron transfer (charge recombination) kinetics? Because the optical properties are similar for PE1 and PE4 (Figure 4), we propose that interfacial electron transfer occurs through multiple pathways; electron transfer generally occurs through the π-conjugated linker (BET through bond), but in a randomly packed mesoporous environment, some dye molecules near the TiO_2 surface might transport electrons efficiently through space (Scheme 1); evidence for such transfer has been reported.[25] Alternatively, because of the longer PE linker, PE4 might have better chance to be tilted or to even lie closely to the surface of TiO_2 that facilitates the faster BET as we have observed.

3. Concluding Remarks

To investigate the interfacial dynamics of electron transfer in relation to the observed dependence of cell performance on the length of the linker,[3b] we measured the femtosecond transient absorption of dye solutions and TiO_2 films sensitized with two zinc porphyrins (PE1 and PE4). Both solution and thin-film samples were excited at the maxima of the Soret band (λ_{ex} = 430 nm) and Q bands (λ_{ex} = 620 nm) with the probe of the TA spectra via white-light generation. For the thin-film samples, the dynamics of back electron transfer were studied with excitation at 620 nm and detection in two spectral regions: a visible probe (630 nm) provided the kinetics of the recovery of a depleted ground-state population due to charge recombination, and a mid-IR probe (4.9 μm) provided direct evidence for electron transfer occurring at the dye/TiO_2 interface. The transient of the PE1/TiO_2 film shows a single-exponential decay with a large offset (Δ value), whereas the transient of the PE4/TiO_2 film displays a biexponential decay with a small Δ. Because of the existence of the rapid-decay component, the concentration of delocalized electrons (represented by Δ) in PE4/TiO_2 is smaller than that in PE1/TiO_2. As a result, more free delocalized electrons were produced in the PE1/TiO_2 films than in the PE4/TiO_2 films, and this is consistent with the result showing that the photovoltaic performance of the device decreases systematically with increasing length of the linker.[3b] Even though the more rapid BET kinetics and the smaller Δ values involved at the semiconductor/dye interface of the PE4/TiO_2 films might account for that poor cell performance, other factors such as the kinetics involved at the TiO_2/dye/electrolyte interface (interception of the electrons in the conduction band of TiO_2 with tri-iodide anions in the electrolyte) were not considered in the present work. Experiments in progress will produce further evidence for the photovoltaic performance of the device decreasing systematically with increasing length of the linker.

4. Experimental Section

4.1. Sample Preparation and Steady-State Spectral Measurements. PE1 and PE4 were synthesized with the standard Sonogashira cross-coupling methods.[3,26] TiO_2 nanoparticle films were prepared as reported elsewhere.[3,27] The thickness of the TiO_2 film was 6 μm; the particle size was 15−20 nm. The dye-sensitized TiO_2 films were prepared on soaking the TiO_2 film in a dye/THF/CH_2Cl_2 solution (10^{-4} M, THF:CH_2Cl_2 = 1:14) for 8 h, and washed with clean acetonitrile to remove all materials not chemically adsorbed onto the TiO_2 film. For fs TA experiments, the sensitized TiO_2 films were immersed in acetonitrile in a rotary quartz cell to mimic the environment of the dye in a device with the presence of polar solvent molecules. UV/visible absorption spectra of samples in solution and thin films were measured with a standard spectrometer (Cary 50, Varian). Emission spectra were obtained with a composite CCD spectrometer (USB2000FLG, Ocean Optics) with an excitation source shared with the femtosecond laser system used in time-resolved measurements.

4.2. Femtosecond Vis/NIR Transient Absorption Measurements. The femtosecond transient absorption measurements were performed with an ultrarapid amplified system described elsewhere.[25b] Briefly, the regenerative amplifier (Legend USP-1K-HE) was pumped with a Nd:YLF laser (1 kHz, Evolution 30, Coherent). The regenerative amplifier generated a femtosecond pulse centered at 800 nm, and the average peak power was 2.5 mJ $pulse^{-1}$. The width of the amplified pulse at 800 nm was 60 fs, as determined with a single-shot autocorrelator (SSA, Coherent). The amplified pulse was used to pump two optical parametric amplifiers (OPerA-F, Coherent). For visible and near-IR transient absorption experiments, the generated signal and idler pulse were sent to a harmonic generation module, which provided light tunable from 300 to 1500 nm.

The sensitizers' stability on TiO_2 films was tested based on a scan of the TA profiles, for which the successful TA decay traces should be reproducible within the experimental uncertainties during the scan. For the thin-film samples excited at the 620 nm, the reproducibility of the scan of the TA traces was excellent. However, signal degradation occurred when the sensitizers were excited at 430 nm repeatedly, and this problem was solved by attenuation of the power of the pump pulse until the degradation was minimized. In addition, the position of the laser spot irradiated on the sample was adjusted to a new location in each scan. Accordingly, the powers of the excitation pulses were properly attenuated to 10 and 30 μW for S_2 (λ_{ex} = 430 nm) and S_1 (λ_{ex} = 620 nm) excitations, respectively.

For the vis/NIR transient absorption system (ExciPro, CDP), the relaxation dynamics were obtained through a pump−probe mechanism. The optical delay between the pump and probe beams was controlled with a stepping translational stage. To obtain the difference spectra with and without excitation, we used a chopper to modulate the excitation pulse. The pump pulse was generated with the OPA/wavelength-conversion module. For measurements with the white-light continuum (WL), the residual amplified pulse (800 nm) was focused on a water cell to generate WL, which was split into two parts: one to overlap the excitation pulse as a probe and the other as a reference. Those two beams were collected with two optical fibers connected to a monochromator and detected with two Si photodiode arrays (2 × 1024 channels). For measurements at a single wavelength, the probe pulse at 630 nm was generated from the second harmonic of the signal of another OPA at 1260 nm and detected with two Si photodiodes.

4.3. Femtosecond Mid-IR Transient Absorption Measurements. Figure 9 shows the optical layout of the femtosecond pump−probe transient-absorption spectrometer with mid-IR detection (ExciProIR, CDP). The probe pulse at 4.9 μm was generated as the difference frequency of the signal (1375 nm) and the idler (1913 nm), focused and collimated through the L1-L2 lens pair onto a nonlinear crystal ($AgGaS_2$); both signal and idler were blocked with a color filter. The resulting probe beam was separated into two parts, one reflected to a MCT detector to serve as a reference signal (I_0), and the other focused on the sample cell via L4 and overlapping the pumping beam to produce a probe signal on another MCT detector. A mechanical chopper modulated the pump beam for the probe signal with excitation (I_{pr}) and without excitation (I_{ref}). At a particular temporal delay t, the difference of absorbance between $I_{pr}(t)$ and I_{ref} is expressible as

$$\Delta OD(t) = OD_1(t) - OD_2 = \log \frac{I_0}{I_{pr}(t)} - \log \frac{I_0}{I_{ref}} = \log \frac{I_{ref}}{I_{pr}(t)} \quad (1)$$

in which $OD_1(t)$ and OD_2 represent the absorbances of the system with excitation and without excitation, respectively. On varying the temporal delay between excitation and probe pulses via a stepping translational stage (delay line), we obtained a transient absorption profile (ΔOD vs t).

Acknowledgment. National Science Council of Taiwan (contracts 94-2120-M-009-004, 96-2628-M-009-018-MY2 and

97-3114-M-009-093-) and the MOE-ATU program provided financial support.

Supporting Information Available: Details on spectral evidence of oxidized porphyrin species and theoretical fits of the kinetic data shown in Figures 7 and 8. This material is available free of charge via the Internet at http://pubs.acs.org.

References and Notes

(1) (a) O'Regan, B.; Grätzel, M. *Nature* **1991**, *353*, 737. (b) Nazeeruddin, M. K.; Kay, A.; Rodicio, I.; Humphry-Baker, R.; Müller, E.; Liska, P.; Vlachopoulos, N.; Grätzel, M. *J. Am. Chem. Soc.* **1993**, *115*, 6382. (c) Hagfeldt, A.; Grätzel, M. *Chem. Rev.* **1995**, *95*, 49. (d) Hagfeldt, A.; Grätzel, M. *Acc. Chem. Res.* **2000**, *33*, 269. (e) Grätzel, M. *Nature* **2001**, *414*, 338.

(2) (a) Wang, Q.; Ito, S.; Grätzel, M.; Fabregat-Santiago, F.; Mora-Seró, I.; Bisquert, J.; Bessho, T.; Imai, H. *J. Phys. Chem. B* **2006**, *110*, 25210. (b) Wei, M.; Konishi, Y.; Zhou, H.; Yanagida, M.; Sugihara, H.; Arakawa, H. *J. Mater. Chem.* **2006**, *16*, 1287. (c) Koide, N.; Islam, A.; Chiba, Y.; Han, L. *J. Photochem. Photobiol. A* **2006**, *182*, 296.

(3) (a) Luo, L.-Y.; Lo, C.-F.; Lin, C.-Y.; Chang, I.-J.; Diau, E. W.-G. *J. Phys. Chem. B* **2006**, *110*, 410. (b) Lin, C.-Y.; Lo, C.-F.; Luo, L.; Lu, H.-P.; Hung, C.-S.; Diau, E. W.-G. *J. Phys. Chem. C* **2009**, *113*, 755–764.

(4) Tachibana, Y.; Moser, J. E.; Grätzel, M.; Klug, D. R.; Durrant, J. R. *J. Phys. Chem.* **1996**, *100*, 20056.

(5) (a) Asbury, J. B.; Hao, E.; Wang, Y.; Ghosh, H. N.; Hirendra, N. G.; Lian, T. *J. Phys. Chem. B* **2001**, *105*, 4545. (b) Anderson, N. A.; Ai, X.; Lian, T *J. Phys. Chem. B* **2003**, *107*, 14414. (c) Anderson, N. A.; Lian, T. *Coord. Chem. Rev.* **2004**, *248*, 1231. (d) Ai, X.; Guo, J.; Anderson, N. A.; Lian, T. *J. Phys. Chem. B* **2004**, *108*, 12795. (e) Anderson, N. A.; Lian, T. *Annu. Rev. Phys. Chem.* **2005**, *56*, 491.

(6) (a) Benkö, G.; Kallioninen, J.; Korppi-Tommola, J. E. I.; Yartsev, A. P.; Sundström, V. *J. Am. Chem. Soc.* **2002**, *124*, 489. (b) Pan, J.; Xu, Y.; Sun, L.; Sundström, V.; Polívka, T. *J. Am. Chem. Soc.* **2004**, *126*, 3066. (c) Benkö, G.; Kallioninen, J.; Myllyperkiö, P.; Trif, F.; Korppi-Tommola, J. E. I.; Yartsev, A. P.; Sundström, V. *J. Phys. Chem. B* **2004**, *108*, 2862. (d) Kallioninen, J.; Benkö, G.; Myllyperkiö, P.; Khriachtchev, L.; Skårman, B.; Wallenberg, R.; Tuomikoski, M.; Korppi-Tommola, J.; Sundström, V.; Yartsev, A. P. *J. Phys. Chem. B* **2004**, *108*, 6365.

(7) Kuciauskas, D.; Monat, J. E.; Villahermosa, R.; Gray, H. B.; Lewis, N. S.; McCusker, J. K. *J. Phys. Chem. B* **2002**, *106*, 9347.

(8) (a) Haque, S. A.; Tachibana, Y.; Klug, D. R.; Durrant, J. R. *J. Phys. Chem. B* **1998**, *102*, 1745. (b) Bach, U.; Tachibana, Y.; Moser, J.-E.; Haque, S. A.; Durrant, J. R.; Grätzel, M.; Klug, D. R. *J. Am. Chem. Soc.* **1999**, *121*, 7445. (c) Tachibana, Y.; Haque, S. A.; Mercer, I. P.; Durrant, J. R.; Klug, D. R. *J. Phys. Chem. B* **2000**, *104*, 1198. (d) Haque, S. A.; Tachibana, Y.; Willis, R. L.; Moser, J. E.; Grätzel, M.; Klug, D. R.; Durrant, J. R. *J. Phys. Chem. B* **2000**, *104*, 538. (e) Durrant, J. R.; Haque, S. A.; Palomares, E. *Coord. Chem. Rev.* **2004**, *248*, 1247. (f) Green, A. N. M.; Palomares, E.; Haque, S. A.; Kroon, J. M.; Durrant, J. R. *J. Phys. Chem. B* **2005**, *109*, 12525. (g) Haque, S. A.; Palomares, E.; Cho, B. M.; Green, A. N. M.; Hirata, N.; Klug, D. R.; Durrant, J. R. *J. Am. Chem. Soc.* **2005**, *127*, 3456.

(9) Hasselmann, G. M.; Meyer, G. J. *J. Phys. Chem. B* **1999**, *103*, 7671.

(10) Heimer, T. A.; Heilweil, E. J. *J. Phys. Chem. A* **2000**, *104*, 4256.

(11) Kuciauskas, D.; Freund, M. S.; Gary, H. B.; Winkler, J. R.; Lewis, N. S. *J. Phys. Chem. B* **2001**, *105*, 392.

(12) Matylitsky, V. V.; Lenz, M. O.; Wachtveitl, J. *J. Phys. Chem. B* **2006**, *110*, 8372.

(13) (a) Ramakrishna, G.; Jose, D. A.; Kumar, D. K.; Das, A.; Palit, D. K.; Ghosh, H. N. *J. Phys. Chem. B* **2005**, *109*, 15445. (b) Ramakrishna, G.; Verma, S.; Jose, D. A.; Kumar, D. K.; Das, A.; Palit, D. K.; Ghosh, H. N. *J. Phys. Chem. B* **2006**, *110*, 9012.

(14) (a) Nazeeruddin, M. K.; Humphry-Baker, R.; Officer, D. L.; Campbell, W. M.; Burrell, A. K.; Grätzel, M. *Langmuir* **2004**, *20*, 6514. (b) Campbell, W. M.; Burrell, A. K.; Officer, D. L.; Jolley, K. W. *Coord. Chem. Rev.* **2004**, *248*, 1363. (c) Wang, Q.; Campbell, W. M.; Bonfantani, E. E.; Jolley, K. W.; Officer, D. L.; Walsh, P. J.; Gordon, K.; Humphry-Baker, R.; Nazeeruddin, M. K.; Grätzel, M. *J. Phys. Chem. B* **2005**, *109*, 15397. (d) Campbell, W. M.; Jolley, K. W.; Wagner, P.; Wagner, K.; Walsh, P. J.; Gordon, K.; Schmidt-Mende, L.; Nazeeruddin, M. K.; Wang, Q.; Pechy, P.; Renouard, T.; Zakeeruddin, S. M.; Grätzel, M.; Officer, D. L. *J. Phys. Chem. C* **2007**, *111*, 11760.

(15) (a) Galoppini, E. *Coord. Chem. Rev.* **2004**, *248*, 1283. (b) Rochford, J.; Chu, D.; Hagfeldt, A.; Galoppini, E. *J. Am. Chem. Soc.* **2007**, *129*, 4655.

(16) (a) Eu, S.; Hayashi, S.; Umeyama, T.; Oguro, A.; Kawasaki, M.; Kadota, N.; Matano, Y.; Imahori, H. *J. Phys. Chem. C* **2007**, *111*, 3528. (b) Hayashi, S.; Matsubara, Y.; Eu, S.; Hayashi, H.; Umeyama, T.; Matano, Y.; Imahori, H. *Chem. Lett.* **2008**, *37*, 846. (c) Eu, S.; Hayashi, S.; Umeyama, T.; Matano, Y.; Araki, Y.; Imahori, H. *J. Phys. Chem. C* **2008**, *112*, 4396. (d) Hayashi, S.; Tanaka, M.; Hayashi, H.; Eu, S.; Umeyama, T.; Matano, Y.; Araki, Y.; Imahori, H. *J. Phys. Chem. C* **2008**, *112*, 15576.

(17) Park, J. K.; Lee, H. R.; Chen, J.; Shinokubo, H.; Osuka, A.; Kim, D. *J. Phys. Chem. C* **2008**, *112*, 16691.

(18) Lee, C.-W.; Lu, H.-P.; Lan, C.-M.; Huang, Y.-L.; Liang, Y.-R.; Yen, W.-N.; Liu, Y.-C.; Lin, Y.-S.; Diau, E. W.-G.; Yeh, C.-Y. *Chem. Eur. J.* **2009**, *115*, 1403.

(19) Lo, C.-F.; Luo, L.; Diau, E. W.-G.; Chang, I.-J.; Lin, C.-Y. Chem. Commun. 2006, *1430*.

(20) (a) Ghosh, H. N. *J. Phys. Chem. B* **1999**, *103*, 10382. (b) Ramakrishna, G.; Ghosh, H. N.; Singh, A. K.; Palit, D. K.; Mittal, J. P. *J. Phys. Chem. B* **2001**, *105*, 12786. (c) Ramakrishna, G.; Singh, A. K.; Palit, D. K.; Ghosh, H. N. *J. Phys. Chem. B* **2004**, *108*, 1701. (d) Ramakrishna, G.; Singh, A. K.; Palit, D. K.; Ghosh, H. N. *J. Phys. Chem. B* **2004**, *108*, 4775.

(21) (a) Asbury, J. B.; Anderson, N. A.; Hao, E.; Ai, X.; Lian, T. *J. Phys. Chem. B* **2003**, *107*, 7376. (b) Guo, J.; She, C.; Lian, T. *J. Phys. Chem. C* **2007**, *111*, 8979.

(22) (a) Gao, Y. Q.; Georgievskii, Y.; Marcus, R. A. *J. Chem. Phys.* **2000**, *112*, 3358. (b) Gosavi, S.; Marcus, R. A. *J. Phys. Chem. B* **2000**, *104*, 2067. (c) Gao, Y. Q.; Marcus, R. A. *J. Chem. Phys.* **2001**, *113*, 6351.

(23) Durrant, J. R.; Haque, S. A.; Palomares, E. *Coord. Chem. Rev.* **2004**, *248*, 1247.

(24) (a) Nelson, J. *Phys. Rev. B* **1999**, *59*, 374. (b) Nelson, J.; Haque, S. A.; Klug, D. R.; Durrant, J. R. *Phys. Rev. B* **2001**, *63*, 205321.

(25) (a) Luo, L.; Chang, C.-W.; Lin, C.-Y.; Diau, E. W.-G. *Chem. Phys. Lett.* **2006**, *432*, 452. (b) Chang, C.-W.; Chou, C. K.; Chang, I.-J.; Lee, Y.-P.; Diau, E. W.-G. *J. Phys. Chem. C* **2007**, *111*, 13288.

(26) Sonogashira, K.; Tohda, Y.; Hagihara, N. *Tetrahedron Lett.* **1975**, *16*, 4467.

(27) Barbé, C. J.; Arendse, F.; Comte, P.; Jirousek, M.; Lenzmann, F.; Shklover, V.; Grätzel, M. *J. Am. Ceram. Soc.* **1997**, *80*, 3157.

JP810580U